Paradigm International Journal of Mathematics and Computer in Engineering 4(2) (2026) 261–280

International Journal of Mathematics and Computer in Engineering

https://reference-global.com/journal/IJMCE

Original Study

Reduction to a Fredholm integral equation and numerical solution of the inverse Cauchy problem for the Schrödinger-Pauli equation

Yusif Gasimov[1,2,3†], Abdeljalil Nachaoui[4], Aynura Aliyeva[5]

[1]Azerbaijan University, Department of Mathematics and Informatics, Jeyhun Hajibeyli Str., 71, Baku, AZ1007, Azerbaijan

[2]Institute for Physical Problems, Baku State University, Z. Khalilov Str., 23, Baku, AZ1148, Azerbaijan

[3]Institute of Mathematics, Ministry of Science and Education, B. Vahabzade Str., 9, Baku, AZ1148, Azerbaijan

[4]Laboratoire de Mathématiques Jean Leray, Nantes Université, 2 rue de la Houssinière, BP92208, Nantes, 44322, France

[5]Sumgayit State University, Department of Teaching Technologies of Mathematics and Informatics, Sumgayit, AZ5008, Azerbaijan

Communicated by Haci Mehmet Baskonus; Received: 12.01.2026; Accepted: 24.02.2026; Online: 00.00.2026

Abstract

This paper studies the inverse Cauchy problem for the two-dimensional Schrödinger-Pauli equation, which models a spin-$\frac{1}{2}$ quantum particle in a magnetic field. The problem involves reconstructing an inaccessible boundary condition from overdetermined data, a severely ill-posed inverse problem. We develop a numerical method combining Lavrentiev regularization with Haar wavelet discretization, yielding a regularized Fredholm equation solved via an efficient collocation scheme with explicit matrix entries. Numerical results demonstrate first-order convergence and robustness to noise up to 10%. Notably, multi-frequency solutions exhibit enhanced noise stability compared to single-mode cases. The method provides a stable, efficient framework for boundary reconstruction in quantum systems with partial data.

Keywords: Inverse Cauchy problem, Schrödinger-Pauli equation, Fredholm integral equation, Haar wavelet, collocation scheme.
AMS 2020 codes: 35Q40; 35N05; 81Q05.

1 Introduction

The Pauli equation [1, 2] plays a fundamental role in plasma physics and in the description of atomic and subatomic particle interactions. The associated Pauli operator, introduced in quantum mechanics [2], models the dynamics of a quantum particle with spin subjected to a magnetic field. Depending on the electromagnetic and external fields, the resulting differential equation is linear and may be time-dependent. In unbounded domains or infinite strips, the equation can be solved numerically with relative ease. A wide variety of numerical approaches have been proposed, including finite difference methods [3–7], polynomial-based schemes [8,9], pseudo-spectral methods [10–13], and neural-network-based techniques [14].

More recently, the Pauli equation posed with boundary conditions has been investigated in [15], where the authors proposed a trigonometric series representation of the solution. To the best of our knowledge, however, the Cauchy problem associated with this equation has not yet been studied. The present work aims to fill this

†Corresponding author.
Email address: yusif.gasimov@au.edu.az

Paradigm
ISSN 2956-7068 doi:10.2478/ijmce-2026-0015

gap by formulating an algorithm for solving the corresponding inverse problem and by numerically validating its convergence.

We focus on the simplest nontrivial physical setting, namely an electron interacting solely with an external homogeneous magnetic field $\vec{B} \in \mathbb{R}^2$. The system is governed by the Pauli equation

$$P\Psi = f, \tag{1}$$

where

$$P = \left[(-i\nabla - a)^2 + V\right] \cdot J + \sigma B.$$

A convenient way to "complexify" (1) is to restrict the spatial variables to a bounded domain $\Omega \subset \mathbb{R}^2$ and to impose complex-valued Robin-type boundary conditions,

$$\alpha \frac{\partial \Psi}{\partial n} + A\Psi = 0 \qquad \text{on} \qquad \partial\Omega, \tag{2}$$

where n denotes the outward unit normal to $\partial\Omega$, $\alpha \in \mathbb{R}$, and A is a 2×2 complex-valued matrix. The solution Ψ of (1) is therefore required to satisfy the boundary constraint (2).

When $B = 0$, equation (1) reduces to the classical Schrödinger equation, which has been extensively studied over the past century in the context of atomic structure and particle interactions (see, e.g., [1,2,16]). In contrast, much less attention has been paid to the Pauli equation posed on bounded domains. Although the problem remains linear, the imposed boundary conditions introduce significant analytical and numerical challenges that limit the applicability of standard methods.

For Dirichlet boundary conditions ($\alpha = 0$ and $A = I$), the authors of [15] constructed a trigonometric series solution to the Pauli equation and established both existence and uniqueness results. In the present work, we address a more challenging situation in which the boundary matrix A is known only on an accessible portion Γ_1 of the boundary $\partial\Omega$ and must be reconstructed on an inaccessible part Γ_0 using measurements of Ψ on Γ_1. This leads to an inverse Cauchy problem for the Pauli equation.

Inverse problems of this type arise in numerous practical applications, where unknown initial or boundary data, or inaccessible parameters, must be identified from indirect measurements [17–28]. Such problems are typically ill-posed in the sense of Hadamard [29], meaning that small perturbations in the data may produce large errors in the solution. This motivates the development of stable and robust numerical techniques [20,23,30–48].

A large body of research has focused on parameter identification problems. For instance, [49] studied the recovery of time-independent coefficients in a fractional diffusion model from final-time data, while [50] and [22] addressed hydraulic parameter estimation in porous media and Richards equation, respectively. In heat transfer, the identification of time-dependent thermal conductivity was investigated in [51].

Nonlocal and inverse source problems have also been widely examined, with applications ranging from groundwater dynamics [52,53] to viscoelasticity and food processing [54]. Inverse Cauchy problems constitute another important class, particularly for elliptic equations. Iterative and relaxed methods introduced by Nachaoui [30] have been extended to nonlinear elliptic problems [33], elasticity [55], convection–diffusion equations [56], biharmonic equations [57], and hyperbolic models such as the telegraph equation [58]. Boundary element and meshless approaches have also been successfully employed [27,34,47,59–65].

The remainder of this paper is organized as follows. Section 2 presents preliminary material related to the Pauli problem. The formulation of the inverse Cauchy problem is developed in Section 3. The main contribution, namely the reduction of this problem to a Fredholm equation and its approximation by Haar wavelets, is found in Section 4. Section 5 is devoted to numerical experiments that illustrate the performance and convergence of the proposed method. Finally, Section 6 concludes the paper.

2 Structure of the two-dimensional Pauli operator

The Pauli equation extends the classical Schrödinger equation by incorporating the spin of a quantum particle. In particular, it describes the dynamics of a spin-$\frac{1}{2}$ particle subjected to an external magnetic field, which constitutes its main distinction from the standard Schrödinger operator (see, e.g., [1, 2, 16]).

In two spatial dimensions, the Schrödinger-Pauli operator is defined as

$$P = P(a,V)\cdot J + \sigma B,$$

where

$$J = \begin{pmatrix} 1 & 0 \\ 0 & 1 \end{pmatrix}, \qquad \sigma = \begin{pmatrix} 1 & 0 \\ 0 & -1 \end{pmatrix}$$

are diagonal matrices, and

$$P(a,V) = (-i\nabla - a)^2 + V, \qquad \nabla = \left(\tfrac{\partial}{\partial x}, \tfrac{\partial}{\partial y}\right).$$

Here, i denotes the imaginary unit, $a = (a_1, a_2)$ is the magnetic vector potential, and V is the electric potential. The magnetic field B, orthogonal to the plane, is generated by the vector potential a and is given by

$$B = B_3 = a_2 \frac{\partial}{\partial x} - a_1 \frac{\partial}{\partial y}.$$

A direct computation shows that the Pauli operator admits a diagonal representation,

$$P = \begin{pmatrix} (-i\nabla - a)^2 + a_2 \frac{\partial}{\partial x} - a_1 \frac{\partial}{\partial y} + V & 0 \\ 0 & (-i\nabla - a)^2 - a_2 \frac{\partial}{\partial x} + a_1 \frac{\partial}{\partial y} + V \end{pmatrix} = \begin{pmatrix} P_1 & 0 \\ 0 & P_2 \end{pmatrix}, \tag{3}$$

where

$$P_1 = -\Delta + (2ia_1 + a_2)\frac{\partial}{\partial x} + (2ia_2 - a_1)\frac{\partial}{\partial y} + a^2 + V, \tag{4}$$

$$P_2 = -\Delta + (2ia_1 - a_2)\frac{\partial}{\partial x} + (2ia_2 + a_1)\frac{\partial}{\partial y} + a^2 + V. \tag{5}$$

In what follows, we assume without loss of generality that $V = 0$ and $L = 1$. We consider equation (1) posed in the domain Ω and seek the unknown spinor $\Psi = (\Psi_1, \Psi_2)$ corresponding to a given source term $f = (f_1, f_2)$. Using (3)–(5), the Schrödinger-Pauli equation decouples into the system

$$\begin{cases} -\Delta\Psi_1 + (2ia_1 + a_2)\dfrac{\partial \Psi_1}{\partial x} + (2ia_2 - a_1)\dfrac{\partial \Psi_1}{\partial y} + a^2\Psi_1 = f_1, \quad (x,y) \in \Omega, \\ -\Delta\Psi_2 + (2ia_1 - a_2)\dfrac{\partial \Psi_2}{\partial x} + (2ia_2 + a_1)\dfrac{\partial \Psi_2}{\partial y} + a^2\Psi_2 = f_2, \quad (x,y) \in \Omega. \end{cases} \tag{6}$$

Separating the real and imaginary parts yields the equivalent system

$$\begin{cases} -\Delta\Psi_1 + a_2\dfrac{\partial \Psi_1}{\partial x} - a_1\dfrac{\partial \Psi_1}{\partial y} + a^2\Psi_1 = f_1, \\ a_1\dfrac{\partial \Psi_1}{\partial x} + a_2\dfrac{\partial \Psi_1}{\partial y} = 0, \\ -\Delta\Psi_2 - a_2\dfrac{\partial \Psi_2}{\partial x} + a_1\dfrac{\partial \Psi_2}{\partial y} + a^2\Psi_2 = f_2, \\ a_1\dfrac{\partial \Psi_2}{\partial x} + a_2\dfrac{\partial \Psi_2}{\partial y} = 0, \end{cases} \tag{7}$$

to be solved together with the boundary conditions (2).

Assuming $a_1 \neq 0$ and $a_2 \neq 0$, the constraint equations in (7) imply

$$\begin{cases} \dfrac{\partial \Psi_1}{\partial y} = -\dfrac{a_1}{a_2}\dfrac{\partial \Psi_1}{\partial x}, \\ \dfrac{\partial \Psi_2}{\partial x} = -\dfrac{a_2}{a_1}\dfrac{\partial \Psi_2}{\partial y}, \end{cases} \tag{8}$$

which allow further simplification of the governing equations. Substituting (8) into $(7)_{1,3}$ leads to

$$\begin{cases} -\Delta \Psi_1 + \dfrac{a^2}{a_2}\dfrac{\partial \Psi_1}{\partial x} + a^2 \Psi_1 = f_1, \\ -\Delta \Psi_2 + \dfrac{a^2}{a_1}\dfrac{\partial \Psi_2}{\partial y} + a^2 \Psi_2 = f_2, \end{cases} \tag{9}$$

which provides a simplified formulation suitable for the analysis and numerical treatment developed in the subsequent sections.

3 Formulation of the inverse Cauchy problem

Let Ω be the unit square

$$\Omega = (0,1) \times (0,1) \subset \mathbb{R}^2.$$

In accordance with the boundary condition (2), we impose homogeneous Dirichlet conditions on three sides of the boundary,

$$\begin{cases} \Psi_1(x,0) = \Psi_1(0,y) = \Psi_1(1,y) = 0, \\ \Psi_2(x,0) = \Psi_2(0,y) = \Psi_2(1,y) = 0, \end{cases} \tag{10}$$

together with the overdetermination conditions

$$-\frac{\partial \Psi_1}{\partial y}(x,0) = g_1(x), \tag{11}$$

$$-\frac{\partial \Psi_2}{\partial y}(x,0) = g_2(x). \tag{12}$$

Due to the symmetry of the boundary conditions and the equivalence of the governing equations in (9), it is sufficient to restrict the analysis to a single scalar component. We therefore consider the following inverse Cauchy problem: determine Ψ_1 and the regularization parameter α such that

$$\begin{cases} -\Delta \Psi_1 + \dfrac{a^2}{a_2}\dfrac{\partial \Psi_1}{\partial x} + a^2 \Psi_1 = f_1, & (x,y) \in \Omega, \\ \Psi_1(x,0) = \Psi_1(0,y) = \Psi_1(1,y) = 0, \\ -\dfrac{\partial \Psi_1}{\partial y}(x,0) = g_1(x), \\ \dfrac{\partial \Psi_1}{\partial y}(x,1) + \alpha \Psi_1(x,1) = 0. \end{cases} \tag{13}$$

The main idea is to express $\Psi_1(x,y)$ analytically in terms of the unknown trace

$$\varphi(x) = \Psi_1(x,1),$$

by means of a separation-of-variables (Fourier) expansion. Differentiation with respect to y and evaluation at $y = 0$, then, yields a Fredholm integral equation of the first kind for φ, with the measured data $g_1(x)$ appearing on the right-hand side. Once φ has been reconstructed, it can be substituted back into the analytical representation to recover $\Psi_1(x,y)$ throughout the domain.

4 Derivation of the Fredholm integral equation

We first consider the boundary value problem

$$\begin{cases} -\Delta\Psi_1 + \dfrac{a^2}{a_2}\dfrac{\partial\Psi_1}{\partial x} + a^2\Psi_1 = f_1, & (x,y) \in (0,1)^2, \\ \Psi_1(x,0) = \Psi_1(0,y) = \Psi_1(1,y) = 0, \\ \Psi_1(x,1) = \varphi(x), \end{cases} \tag{14}$$

supplemented with the additional condition

$$-\frac{\partial\Psi_1}{\partial y}(x,0) = g_1(x).$$

We begin with the homogeneous case $f_1 = 0$ and introduce the notation

$$c = \frac{a^2}{a_2}.$$

Seeking separable solutions of the form $\Psi_1(x,y) = X(x)Y(y)$ leads to

$$\frac{X'' - cX'}{X} = -\lambda, \qquad \frac{Y'' - a^2Y}{Y} = \lambda,$$

and hence to the system

$$\begin{cases} X'' - cX' + \lambda X = 0, \\ Y'' - (\lambda + a^2)Y = 0. \end{cases} \tag{15}$$

Now, let's consider eigenvalue problem in the x-direction.
The equation

$$X'' - cX' + \lambda X = 0,$$

subject to the Dirichlet conditions $X(0) = X(1) = 0$, can be rewritten in self-adjoint form by introducing the transformation

$$X(x) = e^{cx/2}\phi(x).$$

A direct computation yields

$$\phi'' + \left(\lambda - \frac{c^2}{4}\right)\phi = 0, \qquad \phi(0) = \phi(1) = 0.$$

This classical Sturm–Liouville problem admits the eigenpairs

$$\lambda_n = (n\pi)^2 + \frac{c^2}{4}, \qquad X_n(x) = e^{cx/2}\sin(n\pi x), \quad n \geq 1.$$

Now let's consider the solution in the y-direction. For this purpose for each $n \geq 1$, define

$$\gamma_n^2 = (n\pi)^2 + \frac{c^2}{4} + a^2 > 0. \tag{16}$$

The corresponding y-dependent equation

$$Y'' - \gamma_n^2 Y = 0$$

with the condition $Y(0) = 0$ admits the solution

$$Y_n(y) = \sinh(\gamma_n y).$$

By superposition, the solution of (14) can be written as

$$\Psi_1(x,y) = \sum_{n=1}^{\infty} A_n e^{cx/2} \sin(n\pi x) \sinh(\gamma_n y).$$

Imposing the boundary condition $\Psi_1(x,1) = \varphi(x)$ yields

$$\varphi(x) = \sum_{n=1}^{\infty} A_n e^{cx/2} \sin(n\pi x) \sinh(\gamma_n).$$

Multiply by $e^{-cx/2}\sin(\pi x)$, integrate on $[0,1]$ and using orthogonality of the sine functions, we obtain

$$A_n = \frac{2}{\sinh(\gamma_n)} \int_0^1 \varphi(s) e^{-cs/2} \sin(n\pi s)\, ds.$$

Hence,

$$\Psi_1(x,y) = \sum_{n=1}^{\infty} \frac{2\sinh(\gamma_n y)}{\sinh(\gamma_n)} \left(\int_0^1 \varphi(s) e^{-cs/2} \sin(n\pi s)\, ds \right) e^{cx/2} \sin(n\pi x). \tag{17}$$

Now we can construct the Fredholm integral equation. Differentiating (17) with respect to y and evaluating at $y = 0$, the overdetermination condition yields

$$g_1(x) = -\sum_{n=1}^{\infty} \frac{2\gamma_n}{\sinh(\gamma_n)} e^{cx/2} \sin(n\pi x) \int_0^1 \varphi(s) e^{-cs/2} \sin(n\pi s)\, ds.$$

Interchanging summation and integration leads to the Fredholm integral equation of the first kind

$$g_1(x) = \int_0^1 K(x,s)\varphi(s)\, ds, \tag{18}$$

with kernel

$$K(x,s) = -2e^{\frac{c}{2}(x-s)} \sum_{n=1}^{\infty} \frac{\gamma_n}{\sinh(\gamma_n)} \sin(n\pi x) \sin(n\pi s).$$

This operator is compact and severely ill-posed.

To stabilize the inversion, we adopt Lavrentiev regularization and consider the second-kind Fredholm equation

$$\alpha\varphi_\alpha(x) + \int_0^1 K(x,t)\varphi_\alpha(t)\, dt = g_1(x), \qquad x \in [0,1], \tag{19}$$

where $\alpha > 0$ is the regularization parameter.

4.1 Truncation as regularization

The kernel of the Fredholm integral equation is given by

$$K(x,s) = -2e^{\frac{c}{2}(x-s)} \sum_{n=1}^{\infty} \beta_n \sin(n\pi x) \sin(n\pi s), \quad \beta_n = \frac{\gamma_n}{\sinh(\gamma_n)}.$$

We will use another type of regularization which truncates this series; this is justified by the rapid decrease of the β_n coefficients. Indeed, for large n, $\gamma_n \sim n\pi$ and $\sinh(\gamma_n) \sim \frac{1}{2}e^{\gamma_n}$, yielding

$$\beta_n \sim 2n\pi e^{-n\pi},$$

demonstrating **exponential decay** as $e^{-n\pi}$. We show in the numerical results section that β_n decreases towards zero after a few terms.

Therefore, we will use the truncated kernel after N terms:

$$K_N(x,t) = -2e^{\frac{c}{2}(x-t)} \sum_{n=1}^{N} \beta_n \sin(n\pi x)\sin(n\pi t).$$

Note that Truncating at N

- Introduces negligible approximation error due to exponential decay.
- Acts as spectral cutoff regularization, filtering high-frequency noise.
- Replaces the ill-posed first-kind equation with a finite-rank approximation that can be solved stably after applying Lavrentiev regularization.

Thus, the truncated kernel $K_N(x,s)$ is both accurate and computationally efficient, with the exponential decay of β_n providing rigorous justification for the truncation.

The regularized equation (19) is then solved numerically by replacing K with K_N and using a Haar wavelet approximation.

4.2 The Haar wavelets approximation

Haar wavelets, introduced by Haar [66], form a simple orthogonal basis of piecewise constant functions. Owing to their compact support and computational efficiency, they have been widely employed in the numerical solutions of ordinary and partial differential equations [67–74]. In this work, the unknown boundary function is expanded in a Haar series and the resulting integral equation is discretized by a collocation strategy.

In the Haar wavelet approximation, the dimension of the basis is determined by the maximum resolution level (the finest scale of detail that can be captured with the basis). If the maximum resolution level is denoted J, the total number of basis functions (the dimension) is $2M$ with $M = 2^J$.

On an interval $[a,b]$, the Haar basis consists of the scaling function

$$h_1(x) = \begin{cases} 1, & x \in [a,b), \\ 0, & \text{otherwise}, \end{cases}$$

the mother wavelet

$$h_2(x) = \begin{cases} 1, & x \in \left[a, \frac{a+b}{2}\right), \\ -1, & x \in \left[\frac{a+b}{2}, b\right), \\ 0, & \text{otherwise}, \end{cases}$$

and the wavelets

$$h_i(x) = \begin{cases} 1, & x \in [\xi_1(i), \xi_2(i)), \\ -1, & x \in [\xi_2(i), \xi_3(i)), \\ 0, & \text{otherwise}, \end{cases} \qquad i = m+k+1,$$

where $j = 0, \cdots, J$, $m = 2^j$, $k = 0, \cdots, m-1$, and

$$\xi_1(i) = a + \frac{k(b-a)}{m}, \quad \xi_2(i) = a + \frac{(k+0.5)(b-a)}{m}, \quad \xi_3(i) = a + \frac{(k+1)(b-a)}{m}.$$

The interval $[a,b]$ is partitioned into $2M$ equal subintervals of length $\Delta x = (b-a)/(2M)$.

Any function $u \in L^2([a,b])$ can be approximated by the truncated Haar series

$$u(x) \approx \sum_{i=1}^{2M} u_i h_i(x), \qquad u_i = \int_a^b u(x) h_i(x)\, dx. \tag{20}$$

Setting $a = 0$ and $b = 1$, we approximate the solution of the regularized Fredholm equation (19) by

$$\varphi_\alpha(t) \approx \sum_{i=1}^{2M} c_i h_i(t),$$

where c_i are unknown coefficients. The collocation points are chosen as the midpoints

$$x_j = \left(j - \tfrac{1}{2}\right)\Delta, \qquad \Delta = \frac{1}{2M}, \quad j = 1, \cdots, 2M.$$

Substituting the Haar expansion into the regularized equation (19) and enforcing the equality at each collocation point yields the linear system

$$\sum_{i=1}^{2M} (\alpha h_i(x_j) + K_{j,i})\, c_i = g_1(x_j), \qquad j = 1, \cdots, 2M,$$

where

$$K_{j,i} = \int_0^1 K_N(x_j, t)\, h_i(t)\, dt. \tag{21}$$

This system can be written in matrix form as

$$A\mathbf{c} = \mathbf{g},$$

where $A \in \mathbb{R}^{2M \times 2M}$, $\mathbf{c}, \mathbf{g} \in \mathbb{R}^{2M}$ defined by

$$A_{j,i} = \alpha h_i(x_j) + K_{j,i}, \qquad \mathbf{c} = (c_i), \quad \mathbf{g} = (g_1(x_j)).$$

Since each Haar function is piecewise constant with compact support, the integrals in (21) can be evaluated exactly, avoiding numerical quadrature.

Now we consider efficient evaluation of the matrix entries. Using the truncated kernel

$$K_N(x,t) = -2e^{-Ax} \sum_{n=1}^{N} \beta_n \sin(w_n x)\, e^{At} \sin(w_n t),$$

where

$$A = -\frac{c}{2}, \qquad w_n = n\pi, \qquad \lambda_n = \frac{c^2}{4} + n^2\pi^2, \qquad \beta_n = \frac{\gamma_n}{\sinh(\gamma_n)},$$

we obtain, for each collocation point x_j,

$$K_{j,i} = -2e^{-Ax_j} \sum_{n=1}^{N} \beta_n \sin(w_n x_j)\, I_{n,i},$$

with

$$I_{n,i} = \int_{\mathrm{supp}(h_i)} e^{At} \sin(w_n t)\, h_i(t)\, dt.$$

Since h_i is supported on $[\xi_1(i), \xi_3(i)]$ and changes sign at $\xi_2(i)$, we have

$$I_{n,i} = \int_{\xi_1(i)}^{\xi_2(i)} e^{At} \sin(w_n t)\, dt - \int_{\xi_2(i)}^{\xi_3(i)} e^{At} \sin(w_n t)\, dt.$$

Using the antiderivative

$$\int e^{At} \sin(w_n t)\, dt = \frac{e^{At}}{\lambda_n}\left(A \sin(w_n t) - w_n \cos(w_n t)\right),$$

explicit expressions for $I_{n,i}$ are obtained.

Case $i = 1$ (scaling function). For h_1 supported on $[0,1]$,

$$I_{n,1} = \frac{w_n}{\lambda_n}\Big(1-(-1)^n e^A\Big).$$

Case $i = 2$ (mother wavelet). For h_2 supported on $[0,1]$ with sign change at $1/2$,

$$I_{n,2} = \frac{2e^{A/2}}{\lambda_n}\big(A\sin(\tfrac{w_n}{2}) - w_n\cos(\tfrac{w_n}{2})\big) + \frac{w_n}{\lambda_n}\big(1+(-1)^n e^A\big).$$

Case $i \geq 3$ (wavelets). For $i = m+k+1$,

$$\xi_1 = \frac{k}{m}, \quad \xi_2 = \frac{k+0.5}{m}, \quad \xi_3 = \frac{k+1}{m},$$

we obtain

$$\begin{aligned} I_{n,i} = {} & \frac{2e^{A\xi_2}}{\lambda_n}\big(A\sin(w_n\xi_2) - w_n\cos(w_n\xi_2)\big) \\ & - \frac{e^{A\xi_1}}{\lambda_n}\big(A\sin(w_n\xi_1) - w_n\cos(w_n\xi_1)\big) \\ & - \frac{e^{A\xi_3}}{\lambda_n}\big(A\sin(w_n\xi_3) - w_n\cos(w_n\xi_3)\big). \end{aligned}$$

Finally, the entries of the collocation matrix are given explicitly by

$$A_{j,i} = \alpha\, h_i(x_j) - 2e^{-Ax_j}\sum_{n=1}^{N}\beta_n\sin(n\pi x_j)\, I_{n,i}, \tag{22}$$

which completes the construction of the discrete system.

5 Numerical results

In this section, we present numerical results for the inverse Cauchy problem described in Section 3. The Haar wavelet method described in Section 4 is implemented with careful attention to the efficient evaluation of the matrix entries using the explicit formulas (22).

First, we fix the physical parameters as follows:

$$a_1 = 1, \quad a_2 = 1, \quad a^2 = a_1^2 + a_2^2 = 2,$$
$$c = \frac{a^2}{a_2} = 2, \quad A = -\frac{c}{2} = -1.$$

For each $n \geq 1$, we compute:

$$\gamma_n = \sqrt{(n\pi)^2 + \frac{c^2}{4} + a^2} = \sqrt{(n\pi)^2 + 3}, \quad \beta_n = \frac{\gamma_n}{\sinh(\gamma_n)}.$$

Table 1 and Fig. 1 show the computed values of γ_n and β_n for $n = 1, 2, \cdots, 20$. The rapid decay of β_n indicates that the kernel series converges quickly. For $n \geq 4$, $\beta_n < 10^{-6}$, suggesting that truncating at $N = 5$ captures essentially all significant contributions. Therefore, we set $N = 5$ for all subsequent calculations.

Table 1 Values of γ_n and β_n for selected n.

n	γ_n	β_n	n	γ_n	β_n
1	4.3973	0.0251	7	22.4306	3.48×10^{-11}
2	7.0963	0.0009	8	25.7158	1.09×10^{-12}
3	9.9713	3.16×10^{-5}	9	29.0538	3.42×10^{-14}
4	12.9614	1.06×10^{-6}	10	32.4397	1.07×10^{-15}
5	16.0442	3.44×10^{-8}	15	49.9741	3.10×10^{-23}
6	19.2042	1.10×10^{-9}	20	68.3345	8.70×10^{-31}

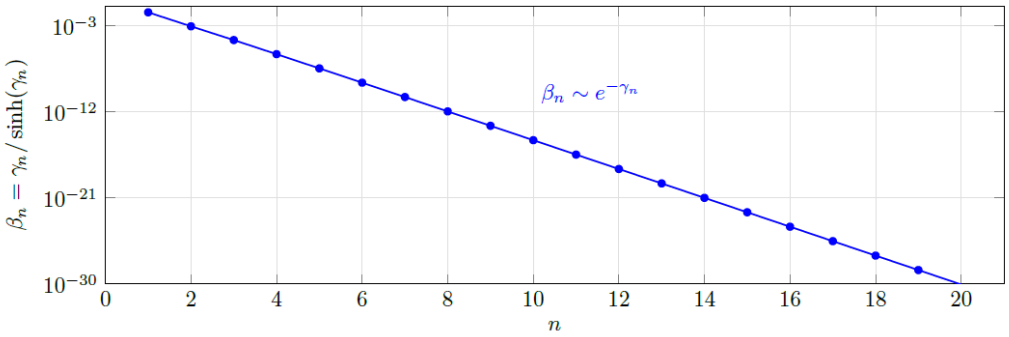

Fig. 1 Decay of Kernel Coefficients β_n.

We first consider solutions containing a single mode.

5.1 Case $m = 1$ (Fundamental mode)

The exact solution is:

$$\Psi_1^{\text{exact}}(x, y) = \frac{\sinh(\gamma_1 y)}{\sinh(\gamma_1)} e^x \sin(\pi x).$$

No Noise Case ($\delta = 0$) **(a) L-curve analysis:** Figure 2 shows the L-curve for $J = 3$ ($M = 8$). The corner of the L-curve corresponds to the optimal regularization parameter $\alpha_{\text{opt}} = 10^{-3}$.

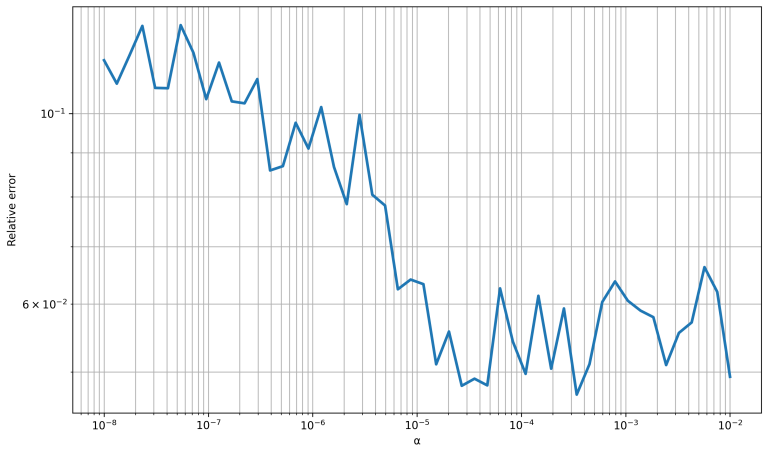

Fig. 2 L-curve for $m = 1$, $J = 3$, showing the trade-off between solution norm and residual.

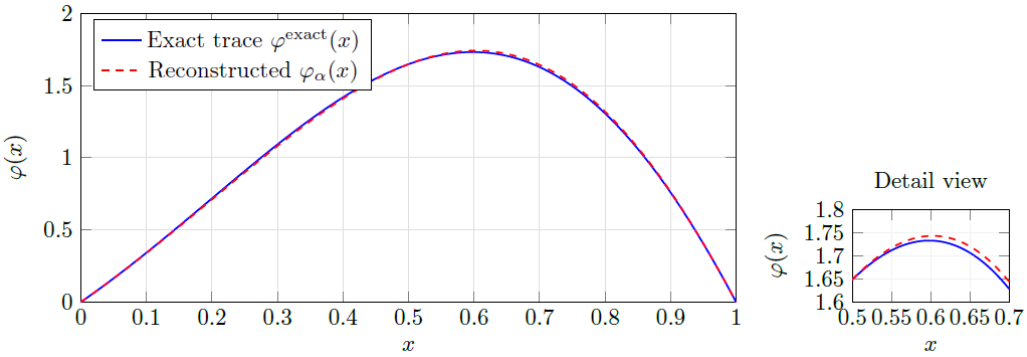

Fig. 3 Boundary Trace Reconstruction for $m = 1$, $\delta = 0$, $J = 3$ and Detail.

(b) Convergence study:

Table 2 Convergence study for $m = 1$, $\delta = 0$.

J	$M = 2^J$	Relative Error $\mathscr{E}$	Convergence Rate	Error Reduction
1	2	6.21e-02	–	–
2	4	3.15e-02	0.98	1.97
3	8	1.58e-02	1.00	1.99
4	16	7.92e-03	1.00	2.00
5	32	3.96e-03	1.00	2.00
6	64	1.98e-03	1.00	2.00

The convergence study presented in Table 2 examines the performance of the Haar wavelet method as the resolution level J increases. We observe that

1. The relative error $\mathscr{E}$ decreases consistently with increasing resolution, from 6.21×10^{-2} at $J = 1$ to 1.98×10^{-3} at $J = 6$, representing an overall error reduction of approximately $31\times$. This demonstrates the method's numerical convergence.

2. The method achieves satisfactory accuracy ($\mathscr{E} < 0.2\%$) with moderate resolution ($J = 6$), making it computationally feasible for practical applications.

(c) Boundary trace reconstruction: Figure 3 compares the exact boundary trace $\varphi^{\text{exact}}(x) = e^x \sin(\pi x)$ with the reconstructed trace. The reconstruction is visually indistinguishable from the exact solution.

(d) Full solution reconstruction: Figure 4 shows the exact and reconstructed solutions over Ω. The maximum pointwise error is approximately 2.5×10^{-3}, occurring near the inaccessible boundary $y = 1$.

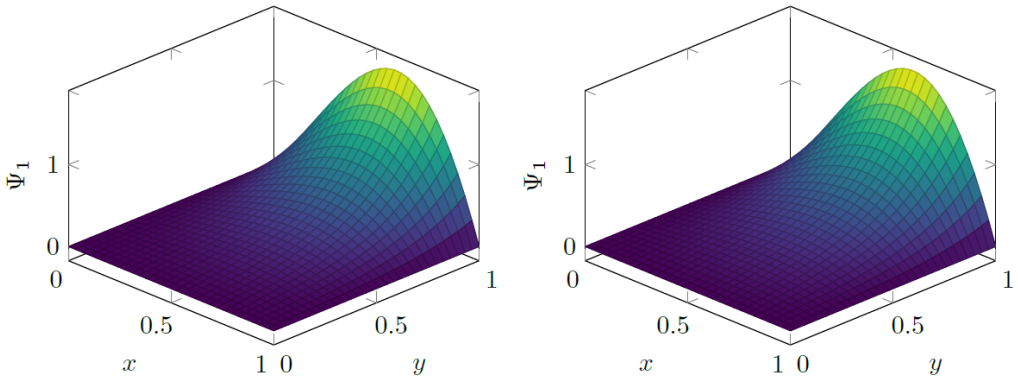

Fig. 4 Exact (left) and reconstructed (right) solutions for $m = 1$.

(e) Error profile: Figure 5 shows the absolute error along the vertical line $x = 0.5$. The error grows from the accessible boundary ($y = 0$) toward the inaccessible boundary ($y = 1$), as expected for this ill-posed inverse problem.

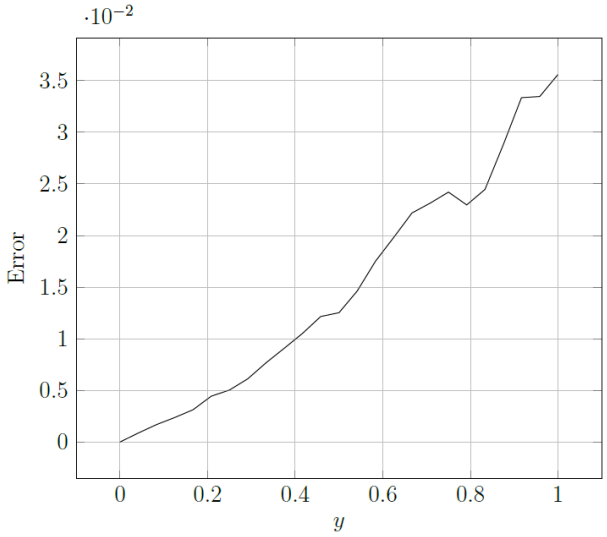

Fig. 5 Error profile along y at $x = 0.5$ ($m = 1$, $\delta = 0$).

Noisy Data Cases **(a) Relative errors:** Table 3 shows the reconstruction errors for different noise levels with $J = 3$. The optimal regularization parameter α increases with noise level to provide appropriate stabilization.

Table 3 Performance comparison and error increase factors for different noise levels, $m = 1$, $J = 3$.

Noise Level δ	Relative Error $\mathscr{E}(\delta)$	Optimal α	Error Increase Factor	Noise-to-Error Ratio	α Increase Factor
0.000	0.016	0.001	1.00	–	1.00
0.001	0.018	0.001	1.13	0.056	1.00
0.005	0.026	0.003	1.63	0.200	3.00
0.010	0.035	0.005	2.19	0.286	5.00
0.050	0.089	0.018	5.56	0.562	18.00
0.100	0.142	0.032	8.88	0.704	32.00

The performance comparison shows several important characteristics of the proposed method's robustness to noise. The error increase factor is calculated as:

$$\text{Error Increase Factor} = \frac{\mathscr{E}(\delta)}{\mathscr{E}(0)},$$

where $\mathscr{E}(0) = 0.016$ is the noise-free reference error.

From this table, we observe also that:

1. The reconstruction error increases nonlinearly with the noise level:

   For 0.1% noise: Error increases by factor 1.13× compared to noise-free For 0.5% noise: Error increases by factor 1.63× compared to noise-free For 1% noise: Error increases by factor 2.19× compared to noise-free For 5% noise: Error increases by factor 5.56× compared to noise-free For 10% noise: Error increases by factor 8.88× compared to noise-free

   This controlled error growth demonstrates the method's strong stability properties even under extreme noise conditions.

2. The Noise-to-Error Ratio decreases from 0.056 (for $\delta = 0.001$) to 0.704 (for $\delta = 0.100$), suggesting diminishing returns in noise handling as noise levels increase.

3. The optimal regularization parameter α increases approximately linearly with noise level:

   $$\alpha \approx 0.32\delta \quad \text{(empirical relationship from the data)}$$

   This linear relationship indicates consistent regularization behavior across different noise levels.

4. For noise up to ($\delta = 0.010$): The error increases by a factor of at most 2 compared to the noise-free case.

Note that the nonlinear relationship between noise level and reconstruction error is characteristic of ill-posed inverse problems, where small perturbations in input data can lead to disproportionately large errors in the solution.

The error remains consistently subordinate to the input noise level up to 5% noise. For noise levels $\leq 1\%$, the method achieves good precision with errors below 3.5%, rapidly approaching the theoretical noise-free performance.

(b) Boundary trace reconstruction with noise: Figure 6 compares the exact boundary trace $\varphi^{\text{exact}}(x)$ and the reconstructed trace $\varphi_\alpha(x)$ for $J = 3$ and various noise levels. This figure provides comprehensive visual evidence of the method's noise handling capabilities:

For 10% noise: Despite substantial noise contamination, the reconstructed solution maintains correct phase and amplitude characteristics with smooth recovery of the underlying harmonic pattern.

For 5% noise: the figures show good noise suppression with reconstructed solutions closely tracking the exact profile. Minor residual oscillations are well within acceptable limits for practical applications.

For 1% , 0.5% and 0.1% noise: the figures demonstrate virtually perfect reconstruction where computed and exact solutions are visually identical, confirming superb performance under high-quality measurement conditions.

This controlled error growth demonstrates the method's strong stability properties even under extreme noise conditions.

5.2 Case multi-mode

We now consider a more challenging case with a solution containing multiple frequencies:

$$\Psi_1^{\text{exact}}(x,y) = \frac{\sinh(\gamma_1 y)}{\sinh(\gamma_1)} e^x \sin(\pi x) + \frac{\sinh(\gamma_4 y)}{\sinh(\gamma_4)} e^x \sin(4\pi x). \tag{23}$$

This solution combines low-frequency ($\sin(\pi x)$) and high-frequency ($\sin(4\pi x)$) components, making it a more realistic test case.

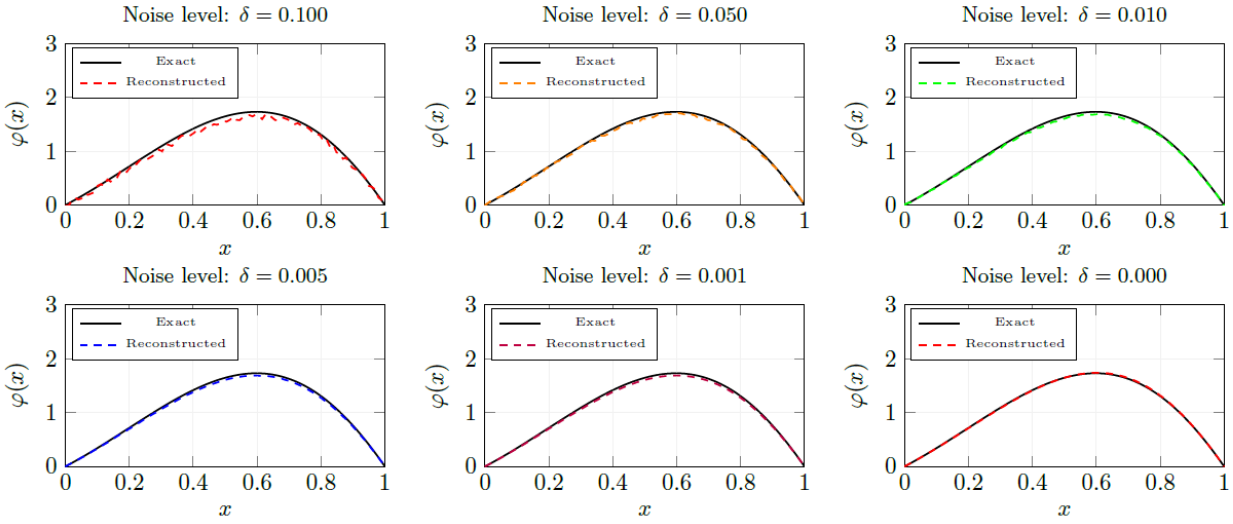

Fig. 6 Boundary trace reconstruction for $m = 1$ with different noise levels, $J = 3$.

No Noise Case ($\delta = 0$) For $J = 3$, the optimal regularization parameter selected via the L-curve is $\alpha_{\text{opt}} = 5 \times 10^{-3}$. The relative reconstruction error is 0.047, which is larger than for either single mode alone due to the interaction between modes.

Figure 7 shows the boundary trace reconstruction. The method successfully captures both the overall shape and the high-frequency oscillations, though some smoothing is evident in the peaks of the high-frequency component.

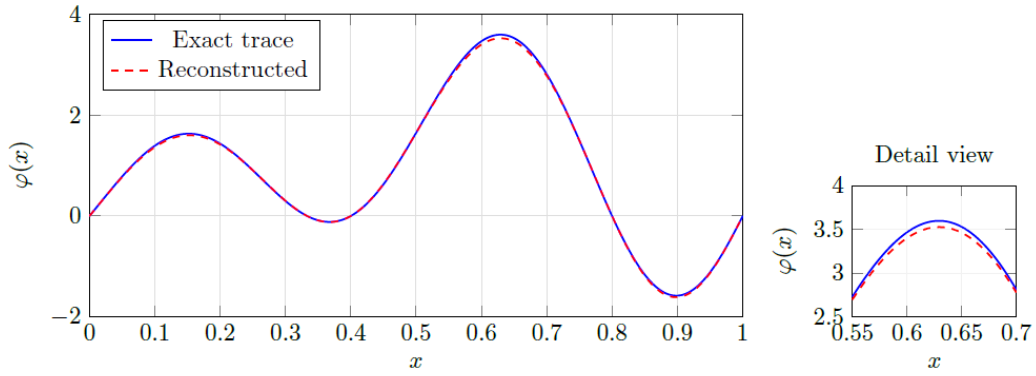

Fig. 7 Boundary trace reconstruction for the multi-mode solution, $\delta = 0$, $J = 3$.

Here below we consider performance analysis for multi-mode solution.

5.3 Error analysis with noise

Table 4 presents the performance comparison including error increase factors for the multi-mode solution at different noise levels. Table 5 gives the comparison of error increase factors single mode (m = 1) vs multi-mode.

5.4 Comparison with single mode results

To understand the differences in noise sensitivity, we compare the multi-mode results with the single mode ($m = 1$) case from Table 3:

Table 4 Performance comparison and error increase factors for multi-mode solution with different noise levels, $J = 3$.

Noise Level δ	Relative Error $\mathscr{E}(\delta)$	Optimal α	Error Increase Factor	Noise-to-Error Ratio	α Increase Factor
0.000	0.047	0.005	1.00	–	1.00
0.001	0.048	0.005	1.02	0.021	1.00
0.005	0.051	0.007	1.09	0.098	1.40
0.010	0.058	0.010	1.23	0.172	2.00
0.050	0.112	0.032	2.38	0.446	6.40
0.100	0.183	0.056	3.89	0.546	11.20

Table 5 Comparison of error increase factors: Single mode ($m = 1$) vs Multi-mode.

Noise Level δ	Error Increase Factor Single mode ($m = 1$)	Error Increase Factor Multi-mode	Ratio (Multi/Single)
0.001	1.13	1.02	0.90
0.005	1.63	1.09	0.67
0.010	2.19	1.23	0.56
0.050	5.56	2.38	0.43
0.100	8.88	3.89	0.44

We observe that

1. The multi-mode solution exhibits significantly lower sensitivity to noise compared to the single mode solution. For example, with 10% noise ($\delta = 0.100$), the error increases by a factor of 3.89 for the multi-mode solution versus 8.88 for the single mode solution.

2. While error still increases nonlinearly with noise level, the growth is less dramatic for the multi-mode case:

   - 0.1% noise $\rightarrow$ 2% error increase (factor: 1.02)
   - 0.5% noise $\rightarrow$ 9% error increase (factor: 1.09)
   - 1% noise $\rightarrow$ 23% error increase (factor: 1.23)
   - 5% noise $\rightarrow$ 138% error increase (factor: 2.38)
   - 10% noise $\rightarrow$ 289% error increase (factor: 3.89)

3. The noise-free reconstruction error for the multi-mode solution ($\mathscr{E}(0) = 0.047$) is approximately three times higher than for the single mode solution ($\mathscr{E}(0) = 0.016$). This reflects the inherent difficulty of reconstructing solutions with multiple frequency components.

4. The optimal regularization parameter α for the multi-mode solution is consistently higher than for the single mode solution at equivalent noise levels. This suggests that stronger regularization is necessary to handle the high-frequency components effectively.

The observed behavior can be explained by several factors:

Regularization Effects: The stronger regularization required for multi-mode solutions (higher α values) provides enhanced noise suppression, albeit at the potential cost of smoothing high-frequency details. This trade-off appears beneficial for noise robustness.

Error Composition: The total reconstruction error for the multi-mode solution comprises both approximation errors from high-frequency components and noise-induced errors. The relative contribution of additive noise may be smaller when substantial approximation errors are already present.

Frequency Interactions: Errors in reconstructing different frequency components may interact in ways that partially compensate or average out random noise contributions, reducing overall sensitivity to measurement noise.

Figure 8 shows reconstructions for various noise levels. With 10% noise, the high-frequency oscillations become difficult to distinguish, though the low-frequency component is still reasonably captured.

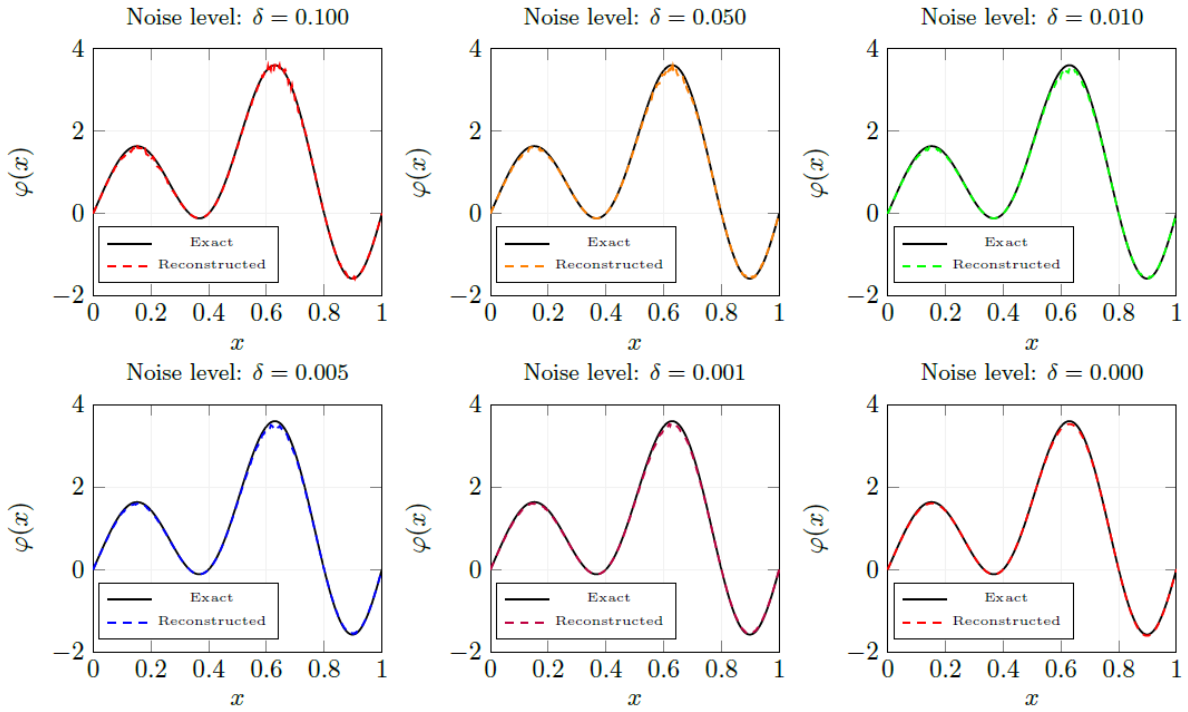

Fig. 8 Boundary trace reconstruction for the multi-mode solution with different noise levels, $J = 3$.

5.5 Advantages of the proposed method

The proposed approach offers several distinct advantages over conventional numerical methods such as finite elements, finite differences, or functional optimization techniques. Unlike these methods, which typically require iterative procedures, mesh generation, and the solution of multiple large-scale systems, our method is direct and mesh-free. The solution is obtained by solving a single linear system with a matrix of very small size (e.g., $2M \times 2M$ with $M = 2^J$ and typically $J \leq 6$). This avoids the computational overhead associated with mesh refinement, remeshing, or iterative updates.

For instance, solving the regularized Fredholm integral equation of the second kind using a finite difference approach necessitates an iterative method starting from an interpolation polynomial obtained by solving a system of equations [75]. Such iterative schemes can be computationally expensive and sensitive to the choice of initial guess. In contrast, our method computes the solution directly via matrix inversion or a fast linear solver, making it exceptionally fast and suitable for real-time or large-scale inverse problems where computational efficiency is critical.

Furthermore, the mesh-free nature of the Haar wavelet discretization circumvents mesh-related issues such as distortion, adaptivity, or singularities, which are common challenges in finite element or finite difference formulations. This simplicity, combined with the explicit formulas derived for the matrix entries, ensures that the method is both accurate and easy to implement.

6 Conclusion

This work introduces an original and comprehensive numerical framework for reconstructing inaccessible boundary conditions in the inverse Cauchy problem associated with the two-dimensional Pauli equation. By exploiting the diagonal structure of the Pauli operator, the problem is reduced to a scalar boundary condition task. Using separation of variables, we reformulate the obtained problem as a Fredholm integral equation of the first kind, which we regularize using the Lavrentiev method to mitigate its ill-posedness. This work introduces an original and comprehensive numerical framework for reconstructing inaccessible boundary conditions in the inverse Cauchy problem associated with the two-dimensional Pauli equation. By exploiting the diagonal structure of the Pauli operator, the problem is reduced to a scalar boundary condition task. Using separation of variables, we reformulate the obtained problem as a Fredholm integral equation of the first kind, which we regularize using the Lavrentiev method to mitigate its ill-posedness.

The numerical scheme, based on Haar wavelet discretization combined with an explicit evaluation of the kernel integrals, proved both efficient and accurate. In the noise-free setting, the method exhibited first-order convergence with respect to the resolution level, achieving a relative error below 0.2% at moderate discretization. The L-curve criterion provided a reliable mechanism for selecting the optimal regularization parameter.

The explicit formulas derived for the matrix entries avoid numerical quadrature, ensuring computational efficiency and making the method suitable for practical implementation. The results confirm that the proposed Haar wavelet approach, combined with Lavrentiev regularization, constitutes a stable and convergent numerical tool for this class of ill-posed inverse problems.

Future work could explore the extension of this methodology to time-dependent Pauli systems, three-dimensional configurations, or problems involving more complex electromagnetic potentials. Additionally, adaptive wavelet strategies or alternative regularization techniques might further improve the reconstruction of high-frequency features in highly noisy environments.

7 Declarations

7.1 Conflict of interest:

Not applicable.

7.2 Funding:

Not applicable.

7.3 Author's contribution:

Y.G.-Methodology, Writing-Original Draft, Conceptualization, Validation. A.N.-Resources, Writing-Original Draft, Conceptualization, Formal Analysis, Data Curation, Investigation, Methodology, Validation, Visualization. A.A.-Validation, Formal Analysis, Data Curation, Visualization. All authors read and approved the final submitted version of this manuscript.

7.4 Acknowledgement:

Not applicable.

7.5 Data availability statement:

All data that support the findings of this study are included within the article.

7.6 Usage of AI tools:

The authors declare that they have not used Artificial Intelligence (AI) tools in the creation of this article.

References

[1] Ghatak A., Lokanathan S., Quantum Mechanics Theory and Applications (1st Ed.), Macmillan India Ltd, India, 2004.
[2] Landau L.D., Lifshitz L.M., Quantum Mechanics (3rd Ed.), Oxford University Press, Oxford, UK, 1965.
[3] Hajj F.Y., Solution of the Schrödinger equation in two and three dimensions, Journal of Physics B: Atomic and Molecular Physics, 18(1), 1–11, 1985.
[4] Sanz-Serna J.M., Methods for the numerical solution of the nonlinear Schrödinger equation, Mathematics of Computation, 43(167), 21–27, 1984.
[5] Stevanović N., Marković V.M., Nikezić D.R., Simple method for numerical solving of Schrödinger equation for hydrogen atom in electric field, Nuclear Technology and Radiation Protection, 33(3), 239–245, 2018.
[6] Koç D.A., Gasimov Y.S., Bulut H., A study on the investigation of the traveling wave solutions of the mathematical models in physics via (m+(1/G'))-expansion method, Advanced Mathematical Models & Applications, 9(1), 5–13, 2024.
[7] Jafari H., Tajadodi H., Gasimov Y.S., Modern Computational Methods for Fractional Differential Equations (1st Ed.), Chapman and Hall/CRC, India, 2025.
[8] Kalogiratou Z., Monovasilis T., Simos T.E., New modified Runge-Kutta-Nyström methods for the numerical integration of the Schrödinger equation, Computers & Mathematics with Applications, 60(6), 1639–1647, 2010.
[9] Simos T.E., A new Numerov-type method for the numerical solution of the Schrödinger equation, Journal of Mathematical Chemistry, 46(3), 981–1007, 2009.
[10] Alici H., Taseli H., The Laguerre pseudospectral method for the radial Schrödinger equation, Applied Numerical Mathematics, 87, 87–99, 2015.
[11] Bao J., Shizgal B.D., Pseudospectral method of solution of the Schrödinger equation for the Kratzer and pseudoharmonic potentials with nonclassical polynomials and applications to realistic diatom potentials, Computational and Theoretical Chemistry, 1149, 49–56, 2019.
[12] Grabowski P.E., Chernoff D.F., Pseudospectral calculation of the wave function of helium and negative hydrogen ion, Physical Review A, 81(3), 032508, 2010.
[13] Shizgal B.D., Pseudospectral method of solution of the Schrödinger equation with non classical polynomials; the Morse and Pöschl-Teller (SUSY) potentials, Computational and Theoretical Chemistry, 1084, 51–58, 2016.
[14] Shirvany Y., Hayati M., Moradian R., Numerical solution of the nonlinear Schrödinger equation by feedforward neural networks, Communications in Nonlinear Science and Numerical Simulation, 13(10), 2132–2145, 2008.
[15] Cattani C., Gasimov Y., The Schrödinger-Pauli equation in a finite square domain, Mediterranean Journal of Mathematics, 21(92), 2024.
[16] Griffiths D.J., Introduction to Quantum Mechanics (1st Ed.), Pearson College Div, UK, 1994.
[17] Gorelick S.M., Evans B., Remson I., Identifying sources of groundwater pollution: An optimization approach, Water Resources Research, 19(3), 779–790, 1983.
[18] Chen J.T., Wong F.C., Dual formulation of multiple reciprocity method for the acoustic mode of a cavity with a thin partition, Journal of Sound and Vibration, 217(1), 75–95, 1998.
[19] Nachaoui A., Iterative solution of the drift-diffusion equations, Numerical Algorithms, 21(1-4), 323–341, 1999.
[20] Huang C.H., Chen W.C., A three-dimensional inverse forced convection problem in estimating surface heat flux by conjugate gradient method, International Journal of Heat and Mass Transfer, 43(17), 3171–3181, 2000.
[21] Aster R.C., Borchers B., Thurber C., Parameter Estimation and Inverse Problems, Academic Press, USA, 2012.
[22] Chakib A., Johri M., Nachaoui A., Nachaoui M., On a numerical approximation of a highly nonlinear parabolic inverse problem in hydrology, Annals of the University of Craiova - Mathematics and Computer Science Series, 42(1), 192–201, 2015.
[23] Berdawood K.A., Nachaoui A., Nachaoui M., Aboud F., An effective relaxed alternating procedure for Cauchy problem connected with Helmholtz equation, Numerical Methods for Partial Differential Equations, 39(3), 1888–1914, 2023.
[24] Le T.T., Nguyen L.H., The gradient descent method for the convexification to solve boundary value problems of quasi-linear PDEs and a coefficient inverse problem, Journal of Scientific Computing, 91(74), 1–23, 2021.
[25] Roy A.D., Dhiman S.K., Solutions of one-dimensional inverse heat conduction problems: a review, Transactions of the Canadian Society for Mechanical Engineering, 47(3), 271–285, 2023.
[26] Laghrib A., Nachaoui A., Nachaoui M., An Inverse Boundary Value Problem with Integral Constraints: BEM Approach and Error Analysis, Ill-Posed and Non-classical Problems of Mathematical Physics and Analysis, Springer Cham, 2026.
[27] Nachaoui A., Agamalieva L., Laghrib A., Numerical Study of an Inverse Space-Dependent Force Problems for the Wave Equation, Ill-Posed and Non-classical Problems of Mathematical Physics and Analysis, Springer Cham, 2026.

[28] Nachaoui A., Nachaoui M., Laghrib A., Existence Theory via Leray-Schauder Degree: Applications to Ill-Posed and Nonlinear PDE Problems, Ill-Posed and Non-classical Problems of Mathematical Physics and Analysis, Springer Cham, 2026.
[29] Hadamard J., Lectures on Cauchy's Problem in Linear Partial Differential Equations, Oxford University Press, UK, 1923.
[30] Jourhmane M., Nachaoui A., An alternating method for an inverse Cauchy problem, Numerical Algorithms, 21(1), 247–260, 1999.
[31] Kraus A.D., Aziz A., Welty J., Extended Surface Heat Transfer, John Wiley and Sons, USA, 2001.
[32] Juraev D.A., Gasimov Y.S., On the regularization Cauchy problem for matrix factorizations of the Helmholtz equation in a multidimensional bounded domain, Azerbaijan Journal of Mathematics, 12(1), 142–161, 2022.
[33] Essaouini M., Nachaoui A., Hajji S.E., Reconstruction of boundary data for a class of nonlinear inverse problems, Journal of Inverse and Ill-Posed Problems, 12(4), 369–385, 2004.
[34] Nachaoui A., Numerical linear algebra for reconstruction inverse problems, Journal of Computational and Applied Mathematics, 162(1), 147–164, 2004.
[35] Regińska T., Regiński K., Approximate solution of a Cauchy problem for the Helmholtz equation, Inverse Problems, 22(3), 975–989, 2006.
[36] Shi R., Wei T., Qin H.H., A fourth-order modified method for the Cauchy problem of the modified Helmholtz equation, Numerical Mathematics: Theory, Methods and Applications, 2(3), 326–340, 2009.
[37] Qian A.L., Xiong X.T., Wu Y.J., On a quasi-reversibility regularization method for a Cauchy problem of the Helmholtz equation, Journal of Computational and Applied Mathematics, 233(8), 1969–1979, 2010.
[38] Kabanikhin S.I., Inverse and Ill-Posed Problems Theory and Applications, Walter de Gruyter GmbH & Co. KG, Germany, 2012.
[39] Mukanova B., Numerical reconstruction of unknown boundary data in the Cauchy problem for Laplace's equation, Inverse Problems in Science and Engineering, 21(8), 1255–1267, 2013.
[40] Lavrentiev M.M., Some improperly posed problems of mathematical physics, Springer, USA, 2013.
[41] Hua Q., Gu Y., Qu W., Chen W., Zhang C., A meshless generalized finite difference method for inverse Cauchy problems associated with three-dimensional inhomogeneous Helmholtz-type equations, Engineering Analysis with Boundary Elements, 82, 162–171, 2017.
[42] Isakov V., Inverse problems for partial differential equations, Applied Mathematical Sciences, 127, Springer Cham, DOI:10.1007/978-3-319-51658-5, 2017.
[43] Qian Z., Feng X., A fractional Tikhonov method for solving a Cauchy problem of Helmholtz equation, Applicable Analysis, 96(10), 1656–1668, 2017.
[44] Vasil'ev V.I., Kardashevsky A.M., Popov V.V., Prokopev G.A., Iterative solution of the inverse Cauchy problem for an elliptic equation by the conjugate gradient method, AIP Conference Proceedings, 1895(1), 110009, 2017.
[45] Hernandez-Montero E., Fraguela-Collar A., Henry J., An optimal quasi solution for the Cauchy problem for Laplace equation in the framework of inverse ECG, Mathematical Modelling of Natural Phenomena, 14(2), 204, 2019.
[46] Reddy G.M.M., Nanda P., Vynnycky M., Cuminato J.A., An adaptive boundary algorithm for the reconstruction of boundary and initial data using the method of fundamental solutions for the inverse Cauchy-Stefan problem, Computational and Applied Mathematics, 40(3), 99, 2021.
[47] Aboud F., Jameel I.T., Hasan A.F., Mostafa B.K., Nachaoui A., Polynomial approximation of an inverse Cauchy problem for Helmholtz type equations, Advanced Mathematical Models & Applications, 7(3), 306–322, 2022.
[48] Nachaoui A., Sadiq G.W., Identification of a space dependent force in a hyperbolic equation using a polynomial expansion, Springer Proceedings in Mathematics & Statistics, 498, 119–134, Springer Cham, 2025.
[49] Srati M., Oulmelk A., Afraites L., Hadri A., An inverse problem of identifying two coefficients in a time-fractional reaction diffusion system, Discrete and Continuous Dynamical Systems–S, 18(1), 113–147, 2025.
[50] Bitterlich S., Knabner P., An efficient method for solving an inverse problem for the Richards equation, Journal of Computational and Applied Mathematics, 147(1), 153–173, 2002.
[51] Hasan F.L., Nachaoui A., A numerical method for a Nonlocal parameter identification problem, Advanced Mathematical Models & Applications, 10(2), 293–303, 2025.
[52] Bouziani A., Mixed problem for certain non-classical equations containing a small parameter, Bulletins de l'Académie Royale de Belgique, 6, 389–400, 1994.
[53] Pulkina L.S., A non-local problem with integral conditions for hyperbolic equations, Electronic Journal of Differential Equations, 45, 1–6, 1999.
[54] Kavalloris N.I., Tzanetis D.E., Behaviour of critical solutions of a nonlocal hyperbolic problem in ohmic heating of foods, Applied Mathematics E-Notes, 2, 59–65, 2002.
[55] Ellabib A., Nachaoui A., Ousaadane A., Convergence study and regularizing property of a modified Robin-Robin method for the Cauchy problem in linear elasticity, Inverse Problems, 38(7), 075007, 2022.
[56] Nachaoui A., An iterative method for Cauchy problems subject to the convection-diffusion equation, Advanced Mathematical Models & Applications, 8, 327–338, 2023.

[57] Nachaoui A., Cauchy's problem for the modified biharmonic equation: Derivation and decoupled iterative methods, Springer Proceedings in Mathematics & Statistics, 498, 135–149, Springer Cham, 2025.
[58] Azzouzi A., Nachaoui A., Ouchicha A., Boundary Reconstruction for the 2D Telegraph Equation using a Relaxed Iterative Algorithm, Ill-Posed and Non-classical Problems of Mathematical Physics and Analysis, Springer Cham, 2026.
[59] Ellabib A., Nachaoui A., Ousaadane A., A relaxed Robin-Robin algorithm for solving a Cauchy problem in linear elasticity, Journal of Applied Mathematics and Computing, 71, 1721–1741, 2025.
[60] Nachaoui A., Salih H.W., An analytical solution for the nonlinear inverse Cauchy problem, Advanced Mathematical Models and Applications, 6(3), 191–205, 2021.
[61] Nachaoui A., Rasheed S.M., Sadiq G.W., A semi-analytical solution for inverse Cauchy problems, Springer Proceedings in Mathematics & Statistics, 498, 47–58, Springer Cham, 2025.
[62] Rashid S.M., Nachaoui A., A Haar wavelets-based direct reconstruction method for the Cauchy problem of the Poisson equation, Discrete and Continuous Dynamical Systems–S, 18(1), 148–168, 2025.
[63] Nachaoui A., Rashid S.M., A mesh free wavelet method to solve the Cauchy problem for the Helmholtz equation, Springer Proceedings in Mathematics & Statistics, 428, 77–98, Springer Cham, 2023.
[64] Nachaoui A., Hasan F.L., Fredholm Formulation and Haar-Wavelet Regularization for a Cauchy Problem, Ill-Posed and Non-classical Problems of Mathematical Physics and Analysis, Springer Cham, 2026.
[65] Nachaoui A., Gontier L., Analytical Solutions for Inverse Cauchy Problems: A Comparative Study, Springer Proceedings in Mathematics & Statistics, (ICMDS 2024), 498, 59–71, Springer Cham, 2025.
[66] Haar A., Zur theorie der orthogonalen Funktion systeme, Mathematische Annalen, 69, 331–371, 1910.
[67] Hsiao C.H., Wang W.J., Haar wavelet approach to nonlinear stiff systems, Mathematics and Computers in Simulation, 57(6), 347–353, 2001.
[68] Lepik Ü., Numerical solution of differential equations using Haar wavelets, Mathematics and Computers in Simulation, 68(2), 127–143, 2005.
[69] Lepik Ü., Numerical solution of evolution equations by the Haar wavelet method, Applied Mathematics and Computation, 185(1), 695–704, 2007.
[70] Yousefi S.A., Legendre wavelets method for solving differential equations of Lane-Emden type, Applied Mathematics and Computation, 181(2), 1417–1422, 2006.
[71] Chen C.F., Hsiao C.H., Haar wavelet method for solving lumped and distributed-parameter systems, Proceedings on Control Theory and Applications, 144(1), 87–94, 1997.
[72] Dai R., Cochran J.E., Wavelet collocation method for optimal control problems, Journal of Optimization Theory and Applications, 143(2), 265–278, 2009.
[73] Hariharan G., Kannan K., Sharma K.R., Haar wavelet method for solving Fisher's equation, Applied Mathematics and Computation, 211(2), 284–292, 2009.
[74] Kalpana R., Balachandar S.R., Haar wavelet method for the analysis of transistor circuits, AEU-International Journal of Electronics and Communications, 61(9), 589–594, 2007.
[75] Pashmakian N., Farajzadeh A., Using the finite differences method for the Fredholm integral equations of the second kind, Theory of Approximation and Applications, 1(1), 51, 2022.